Draft. November 29, 1996

Gamma Ray Observations of the Early June 1991 Solar Flares

D.L. Bertsch[1], *B.L. Dingus*[1,7,10], *J.A. Esposito*[1,7], *C.E. Fichtel*[1], *R.C. Hartman*[1], *S.D. Hunter*[1], *G. Kanbach*[2], *D.A. Kniffen*[3], *Y.C. Lin*[4], *J.R. Mattox*[5], *H.A. Mayer-Hasselwander*[2], *P.F. Michelson*[4] *C. v.Montigny*[8], *R. Mukherjee*[1,7,9], *P.L. Nolan*[4], *E. Schneid*[6], *P. Sreekumar*[1,7], *and D.J. Thompson*[1]

ABSTRACT

A class X12 flare on the east limb of the Sun on 1991 June 1 signaled the arrival of active region 6659 that was to produce several very large flares during its disk transit. *EGRET*, the high energy gamma ray detector on the Compton Gamma Ray Observatory, detected four of these events in the energy calorimeter. One flare event, on 1991 June 11, produced high energy emission from 50 to over 1000 MeV that was observed in the spark chamber to persist for over 8 hr. The photon spectral shape and time-scale at high energies presented here suggest that the gamma ray were produced by nuclear interactions as well as by electron bremsstrahlung. The long time-scale of the emission seen in the spark chamber requires either a long time-scale acceleration, or an efficient trapping of previously accelerated particles whose subsequent interactions produce gamma

---

[1]Code 661, NASA/Goddard Space Flight Center, Greenbelt, MD 20771

[2]Max-Planck Institut für Extraterrestrische Physik, D-85748 Garching, Germany

[3]Hampden-Sydney College, P.O. Box 862, Hampden-Sydney, VA 23943

[4]Hansen Experimental Physics Laboratory, Stanford University, Stanford, CA 94305

[5]Department of Physics, University of Maryland, College Park, MD. Present address: Physics Department, Boston University, Boston, MA 02215

[6]Northrop Grumman Corporation, Mail Stop A01-26, Bethpage, NY 11714-3580

[7]Universities Research Association

[8]Landessternwarte Heidelberg-Koenigstuhl, 69117 Heidelberg, Germany

[9]Department of Physics, Rutherford Building, McGill University, 3600 University Street, Montreal H3A 2T8, Canada

[10]Department of Physics, University of Utah, Salt Lake City, UT 84112

rays. Analysis of the data from the energy calorimeter reveal line structure in all four of the flares, indicating nuclear interactions of flare accelerated nucleons. These results, together with the time profiles of the 2.22 and 4.4 MeV fluences for all four flares are presented.

Subject headings: sun:flares–sun:gamma rays–gamma rays:observations

1. Introduction

Solar flares have been known to be capable of producing gamma ray emission with energies above several MeV from the early 1970's. Gamma ray production is understood to involve flare-accelerated charged particle interactions with the ambient solar atmosphere (Lingenfelter et al. 1965, Ramaty, Kozlovsky, and Lingenfelter 1975, Murphy et al. 1987, Ramaty and Murphy 1987, Hua and Lingenfelter 1987). Bremsstrahlung from energetic electrons accelerated by the flare or from the decay of charged pion secondaries produced by nuclear interactions yields gamma rays whose energy spectrum is typically a power law extending to the energies of the primary particles. Proton and heavy ion interactions also produce gamma rays through the decay of neutral pions. The gamma ray energy spectrum for this process has a maximum at 68 MeV, and is distinctly different from the bremsstrahlung spectrum. Additionally, nuclei excited by interactions or those produced in excited states emit gamma ray lines below $\sim 8\,MeV$. Being neutral, gamma rays and neutrons travel directly to the Earth and serve as a direct probe of the flare particle acceleration and storage processes.

Two different concepts for particle acceleration have been proposed, shock acceleration (e.g., Forman, Ramaty, and Zweibel 1986) and second-order stochastic acceleration from turbulent plasma (e.g., Forman, Ramaty, and Zweibel 1986, Miller, Guessoum, and Ramaty 1990, Ryan and Lee, 1991). The transport of the accelerated particles (electrons and nucleons) has been studied in detail. Most of the concepts involve an impulsive acceleration that occurs near the top of a coronal loop (Hua, Ramaty, and Lingenfelter 1989, Miller and Ramaty 1989, Ryan and Lee, 1991) after which the particles propagate in the magnetic field of the loop and lose energy by pitch angle scattering and integrations near the foot points of the loop in the chromosphere and photosphere (e.g., Murphy et al. 1987, and Mandzhavidze and Ramaty 1992a. It is these interactions that produce gamma emission by the processes discussed above.

These modeling efforts have been stimulated and constrained by observations from several spacecraft instruments beginning with the observation of the deuterium line at 2.22 MeV

by the gamma ray monitor on OSO-7 (Chupp et al. 1973). The Gamma Ray Spectrometer experiment on the Solar Maximum Mission (SMM) satellite (Forrest et al. 1980) monitored the Sun from 1980 to 1989 and detected approximately 250 flare events with gamma ray emission above $300\,keV$. Only 25 of these extended to energies above $10\,MeV$, and ~ 6 had detectable emission at $140\,MeV$ – the upper threshold of the instrument (Vestrand 1994). The Hinotori satellite instrument (Okudaira et al. 1981) also observed gamma rays emission from solar flares during its 16 month lifetime beginning in early 1981. Approximately 50 flare events were found with significant gamma ray intensity between 0.21 and $6.7\,MeV$.

Most of the gamma ray flare events observed in these early missions had short time scales on the order of $\sim 1\,s$ and a total duration of about $1\,min$ that are associated with the impulsive acceleration phase. On the other hand, longer time scales of tens of minutes are also found, and these suggest an extended acceleration or a trapping (Yoshimuri et al. 1983, Yoshimuri 1990). Many show narrow and broad nuclear line emission features in addition to the bremsstrahlung continuum indicating the presence of energetic protons and heavy ions in the impulsive phase (Chupp 1984, Forrest and Murphy 1988, Rieger 1991). Others are nearly pure bremsstrahlung (Rieger and Marschhauser 1990). Five of the flares observed by *SMM* had energy spectra that indicted a pion-decay feature superposed on the usual bremsstrahlung shape and appear to have a similar extended emission time profile of over $30\,min$ (Dunphy and Chupp 1994). These flares also exhibited line features, and in addition, neutron emission was observed (Dunphy and Chupp 1991).

More recently, the *GAMMA-1* telescope observed flares on 1991 March 26 and 1991 June 15 (Akimov et al. 1991, Leikov et al. 1993). The energy spectrum in the June 15 event was observed up to $2\,GeV$ and the time scale extended to $2\,hr$. *PHEBUS*'s calorimeter observed the 1991 June 11 event for the energies in the nuclear line region below $10\,MeV$ (Trottet et al. 1993). The four instruments on the Compton Gamma Ray Observatory had only been in operation for two months at the time of the exceptional solar activity in 1991 June. These instruments combined to cover the energy range from the hard x-ray regime to several GeV at significantly greater sensitivity than previous instruments had. *OSSE* (Murphy et al. 1993, Johnson et al. 1993) observed spectra with line features and measured time profiles of line fluences in the 1991 June series of flares. *COMPTEL* observers (Ryan et al. 1992, Ryan et al. 1993, Rank et al. 1993) report on gamma ray and neutron emission from the same series of flares. Preliminary *EGRET* results on line emission have been reported (Schneid et al. 1993) in these flares, and for $> 30\,MeV$ emission in the 1991 June 11 event (Kanbach et al. 1993).

This paper describes the *EGRET* observations of a series of four large flare events that occurred in early 1991 June. All four exhibit similar time profiles in the low energy regime between 1 and 200 MeV with a characteristic flash phase followed by extended emission. The spectra all reveal line emission from neutron capture and excitation throughout each event. One of the events on June 11 produced gamma rays detectable to $2\,GeV$, and this flare event persisted for over $8\,hr$. The implications of these results for the production, storage, and energy release mechanisms of the primary particles is then discussed briefly.

2. EGRET Instrument Description

The *EGRET* instrument on the Compton Gamma Ray Observatory (*CGRO*) is a spark chamber telescope that detects gamma rays in the energy range from 30 to over $30,000\,MeV$. Pair production interactions in the chamber are used to reconstruct the arrival direction of individual gamma rays from the spark chamber coordinate data. The energy of the event is determined by the Total Absorption Shower Counter (*TASC*), a NaI(Tℓ) detector that is $8\,rl$ thick, situated at the bottom of the detector. The instrument is covered with an antico-incidence shield to veto charged particle events, and it has a triggering system comprised of two segmented scintillator planes separated by $0.6\,m$. A time-of-flight measurement insures "downward" moving events in the instrument, and the presence of a signal in the *TASC* usually is a required part of the coincidence configuration. More detailed descriptions of the instrument are given by Hughes et al. 1980, Kanbach et al. 1988, Kanbach et al. 1989, and Hartman et al. 1991.

The instrument properties and response functions are given by Thompson et al. 1993, and only the key aspects are summarized here. The on-axis effective area when the *TASC* is included in the coincidence configuration (the nominal mode) is a maximum at $\sim 300\,MeV$ with a value of $1400\,cm^2$. The effective area decreases significantly with decreasing energy below $100\,MeV$, and it falls slowly with energy for energies above $500\,MeV$. At $10,000\,MeV$, for example, the effective area is $700\,cm^2$. The full field-of-view covers 40° from the detector axis and the efficiency is approximately a gaussian function of polar angle with a HWHM of $\sim 20°$. The point spread function has FWHM angles of 5.7°, 2.0°, and 0.4° at energies of 100, 500, and $10,000\,MeV$ respectively. Energy resolution for spark chamber events has a broad minimum from 400 to $1,000\,MeV$ of $\sim 19\%$ and rises slowly at lower and higher energies. In the low energy omni-directional mode, the *TASC* resolution is 20% over its full range from 1 to $200\,MeV$.

For solar flare studies, three types of data are of interest. When the Sun is within $\sim 35°$ of the instrument axis, photons above $30\,MeV$ may be imaged in the spark chamber. For each photon, the time, energy and arrival direction are recorded, and from this information and the exposure, skymaps of intensity and energy spectra may be produced. The *TASC*, in addition to measuring energies of gamma rays that trigger *EGRET*, has an independent omni-directional mode that accumulates energy spectra in 256 channels that are distributed logarithmically over the energy range from 1 to $200\,MeV$. These spectra are regularly obtained every $32.8\,s$. An additional set of four spectra for shorter integrations may be acquired when triggered by the *BATSE* instrument (also on the CGRO). Because the omni-directional mode does not have an anticoincidence shield, the analysis has to correct for a large background, and when the flare is outside the instrument aperture, the analysis of the *TASC* spectra must also include the effects of propagation through significant spacecraft material. The anticoincidence dome has an effective area of $\sim 5.8\,m^2$ and is sensitive to x-rays above $\sim 20\,keV$. It views a major fraction of the sky not occulted by the spacecraft or the earth. The rate is sampled at intervals of $0.256\,s$ with a dynamic range up to 3 MHz and a typical rate of $\sim 40\,kHz$. The dome provides a very sensitive monitor for flare-associated x-rays.

3. Solar Flare Events

The X-class flares and one M–class flare that occurred in early 1991 June are summarized in Table 1. For the first three flares, the Sun was well outside the 35° aperture of the instrument and was only visible to the anticoincidence dome and to the *TASC* detector. A target of opportunity was declared, and the spacecraft was re-oriented toward the Sun on 1991 June 8 permitting the spark chamber (high energy detector) to view the flares on June 9 and 11. An operational problem caused the instrument to be powered off during the time of the June 15 event so that event was entirely missed. Consequently, only two flares were viewed by the spark chamber, and four were detected by the anticoincidence dome and the *TASC*. The Compton Gamma Ray Observatory is in a low earth orbit with a period of $\sim 93\,min$. Figure 1 shows the useful viewing time permitted by orbital constraints for each flare. Here, the periods of occultation by the earth and the portions of the orbit during the South Atlantic Anomaly where the instrument high voltages are turned off to avoid radiation damage are indicated relative to the time of the flare maxima. Notice that the viewing conditions were poor for almost the entire first hour in the June 1 event, and in the case of the June 15 flare, the first $40\,min$ would have been inaccessible if the instrument had been operational.

Table 1: Energetic Flares in 1991 June

Date 1991	Time Maximum	Active Region	Class†	H-α Location	Angles to CGRO Axis Zenith	Azimuth
June 1	1456	6659	X12	N30>Limb	103°	358°
June 4	0339	6659	X12	N30E70	105°	0°
June 6	0107	6659	X12	N33E44	106°	2°
June 9	0143	6659	X10	N34E04	15°	12°
June 11	0209	6659	X12	N31W17	14°	6°
June 11[a]	2005	6659	M5.3	N28W41	13°	4°
June 15	0821	6659	X12	N33W69	12°	350°

†Class is defined in terms as intensity of 1 to 8 A x-ray flux. X signifies $10^{-4}\,watts/m^2$ and M signifies $10^{-5}\,watts/m^2$ and the number following the letter is a multiplier.

[a]Significantly smaller flare, but gamma ray emission was observed. See text.

Note. — Information in this table is taken from *Solar-Geophysical Data Comprehensive Reports* National Oceanic and Atmospheric Administration, No. 568, Part II, Dec. 1991, pp. 3 ffl.

4. Observations

The observations of the spark chamber in the June 11 event and the measurements from the *TASC* for four of the flares are discussed separately below since the results are independent and the analysis methods are different.

4.1. Spark Chamber Results

As already noted, the first three flares in Table 1 were outside the field of view of the spark chamber. The flare on 1991 June 9 was the smallest among the X–class events in terms of its x-ray emission, being classed X10 (Table 1) and it had excellent visibility (Figure 1). A skymap of emission above 100 MeV for this day shows a weak source at the position of the Sun, but the number of events above the diffuse background is too small to provide meaningful analysis for spectra or event time profile. Significant gamma ray emission was observed in the next major flare on June 11. Figure 2 shows the time history of the emission above 50 MeV as well as the background level determined on the previous day. For the

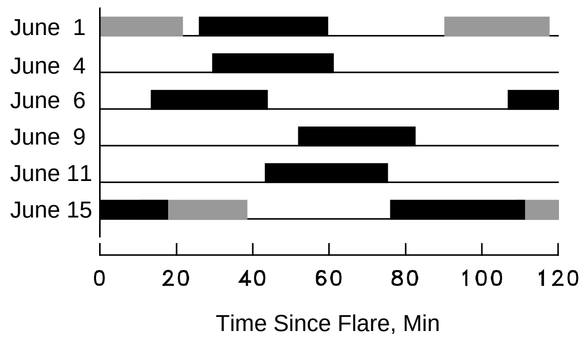

Fig. 1.— The observing times for the flares in 1991 June. Time is measured relative to the flash phase times given in Table 1. The cross-hatched times denote periods when the instrument is in South Atlantic Anomaly region, and the solid bars denote times when the Earth occults the Sun.

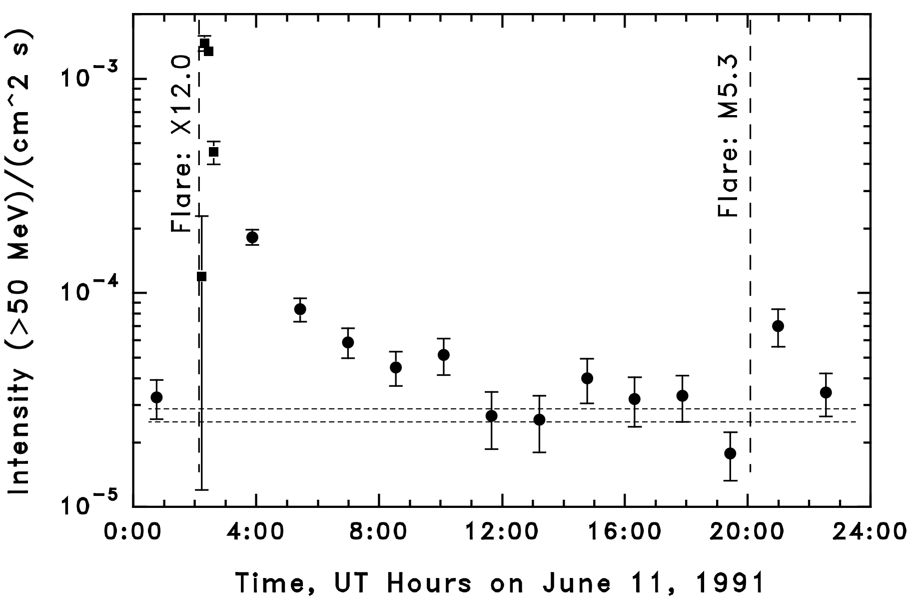

Fig. 2.— Time profile of the gamma ray intensity above 50 MeV. Times are relative to the flash phase times given in Table 1. Circles are from the spark chamber, and squares are from the *TASC*. The dotted lines show the one standard deviation of the background level based on the spark chamber for the previous day. The uncertainties shown are also one standard statistical deviations. The vertical lines denote the times of the X–class and M–class flares in Table 1.

initial $42\,min$ shown in Figure 1, the instrument was unable to trigger on any gamma ray event due to saturation of the anticoincidence counter from solar x-rays above several keV. The anticoincidence count-rate exceeded $3\,MHz$ when typically it only averages $\sim 40\,kHz$. Consequently, the spark chamber could not observe the peak gamma ray flux in the event, and could only begin monitoring solar emission after the end of earth occultation at 03:26 UT. However, the *TASC* detector was able to measure the intensity for $\sim 30\,min$ following the flare. These points are shown as squares in Figure 2. More details of the *TASC* analysis are given in the next section. The intensity above $50\,MeV$ is seen to be above background for at least $8\,hr$ – significantly longer than all previous flare events. Akimov et al. 1991 observed emission above $30\,MeV$ for $2\,hr$ after the June 15 flare, and earlier flares generally had durations of less than $1\,hr$ (e.g., Forrest et al. 1986; Dunphy and Chupp 1991). The long time-scale of this event is likely due to the exceptional size and conditions for cosmic ray production by the Sun, but the greater sensitivity of *EGRET* permitted observations beyond those of other instruments. A significant (3.4σ) increase in intensity following the small M–class flare late in the same day is also evident in Figure 2. This flare occurred in the same solar region, but was separated by $21°$ from the first and it was only $\sim 5\%$ as intense in x-rays (Table 1). In the first five years of the *CGRO* mission, no other M–class event has produced detectable gamma ray emission in the spark chamber. However, the anticoincidence and *TASC* systems detected x-ray and low energy gamma rays from the M5.0 event on 1991 June 30, and from the M4.6 event on 1991 July 2 (Schneid et al. 1996).

The temporal behavior of the June 11 flare high energy emission that could be measured by *EGRET*'s high sensitivity spark chamber telescope extended for $8\,hr$ after the impulsive phase, and was explained by Mandzhavidze and Ramaty 1992b using a model of trapped electrons and protons in coronal loops with a long-term decay in intensity due to collisional losses. The time history observed by *EGRET* in this event allowed estimates of magnetic field strengths, loop sizes and particle pitch angle based on this model. Alternately, adiabatic shock acceleration might account for the observations. The time evolution of the electron and proton source process is perhaps the best discriminator between the two mechanisms.

The photon energy spectrum observed in the *EGRET* spark chamber is shown in Figure 3 for the interval starting at 03:28 UT when the Sun became visible after occultation, and up to 06:00 UT on June 11. The emission is seen to extend to energies of $2\,GeV$. As was noted in an earlier preliminary analysis of the *EGRET* data (Kanbach et al. 1993), the shape of the spectrum suggests that both electron bremsstrahlung and nuclear interaction processes contribute significantly. Model spectra for each of these processes from Mandzhavidze and Ramaty 1992b and Mandzhavidze and Ramaty 1995, based on their thick-target interaction model are shown in Figure 3 along with the sum shown as a solid curve. The two model curves were scaled to produce the best fit to the data. These functions are based on a solar

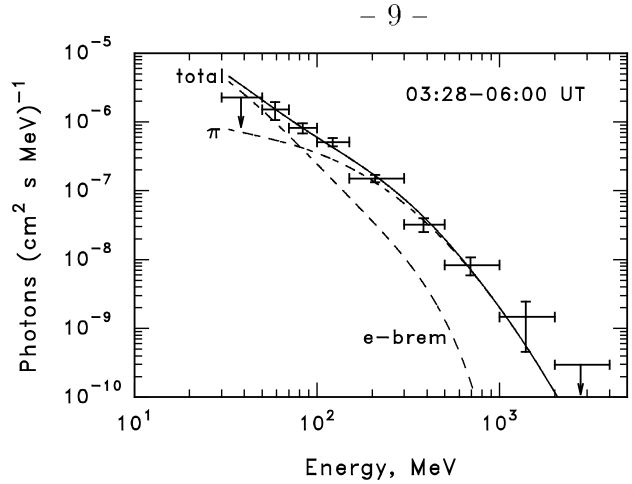

Fig. 3.— Photon differential energy spectrum for the 1991 June 11 flare event. Data were accumulated during the most intense portion from the end of earth occultation at 03:28 UT until 06:00 UT. The dotted curves are from Mandzhavidze and Ramaty 1995 for proton and electron power law spectra of indices −3.0, scaled so that their total, shown as a solid curve, is the best fit to the data. Uncertainties and upper limits are one standard deviation statistical.

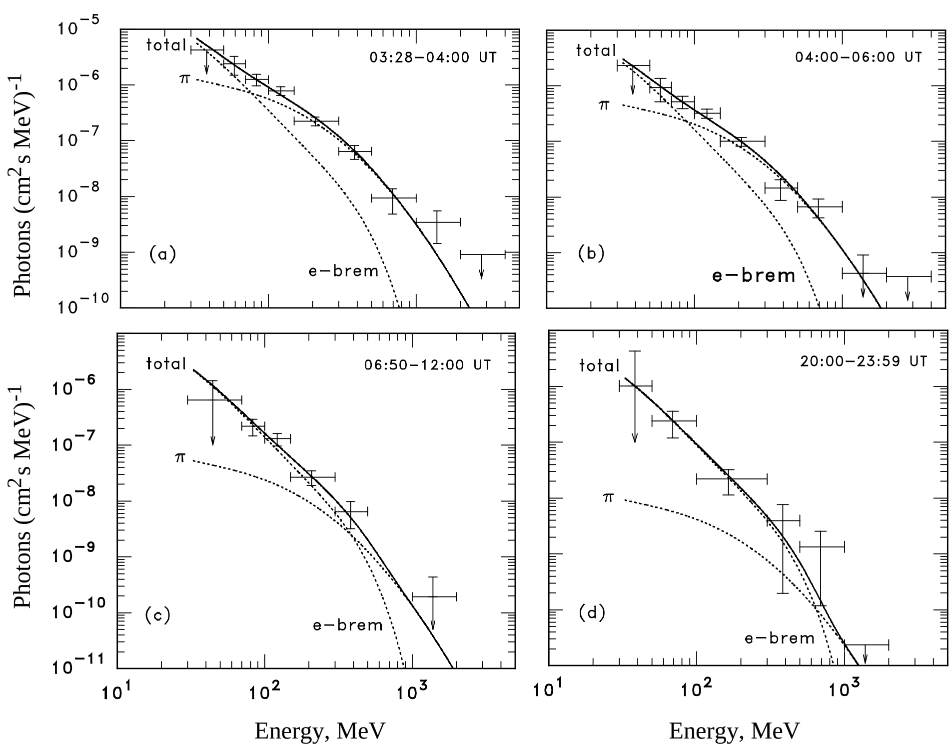

Fig. 4.— Photon differential energy spectra for four selected time periods in the 1991 June 11 solar event. The model curves, described in Figure 3, are fit to the data, and the solid curves are the total emission for the time interval. Uncertainties and upper limits are one standard deviation statistical.

power law spectra with the indexes of -3.0 for the protons and electrons. These values were selected by Mandzhavidze et al. 1996 to fit the *EGRET* data, and since the reduced chi-squared value of the fit is a reasonable 0.89, no other input spectral functions were attempted. By way of comparison, a power law fit to the data in Figure 3 does not fit as well and results in a reduced chi-squared value of 1.94. Akimov et al. 1991 also concluded that both electron and nuclear interactions contributed to the gamma ray spectrum they observed for the June 15 flare event from the same solar region.

The long time-scale of the high energy gamma ray intensity on June 11 raises the interesting question on the solar production mechanisms. If long-term storage is occurring without significant extended acceleration, then the relative contribution from bremsstrahlung should decrease with time since the electrons will lose energy more rapidly than will protons. Figure 4 shows the photon spectra for four time intervals during the event. It is evident that the trend is for the bremsstrahlung contribution to become more significant relative to the pion component as time increases which is the opposite effect to what would be expected for storage. Figure 5 shows the 68% and 95% confidence contours for the bremsstrahlung and pion scale factors for each of the fits in Figure 4. For the first time intervals, both the bremsstrahlung and pion components are significantly non-zero, but in the last two intervals, the pion component may not be significant while the bremsstrahlung component remains significant throughout. The coefficients in these plots are relative to the fitted values in Figure 3. This substantiates the observation in Figure 4 that late in the event, bremsstrahlung is the more significant term. This, somewhat indirect evidence, suggests that an impulsive acceleration and trapping alone cannot account for the time evolution of the gamma ray observations, and that long term or episodic acceleration is required. A similar conclusion was reached by Ramaty and Mandzhavidze 1994, based on the fact that the pion decay gamma emission time profile from *EGRET* is similar to the $2.22\,MeV$ decay profile. In a pure long term trapping model situation, the line profiles would be expected to decay more rapidly (Mandzhavidze and Ramaty 1992b).

4.2. TASC Results

The time history of the energetic flare emission observed by the *EGRET* NaI spectrometer within the first several $1000\,s$ of the impulsive phase varied from flare to flare. Figure 6 shows the high energy (above the line emission region) signals observed by the NaI spectrometer for the 4 flares observed by *EGRET* in 1991 June. Both the June 4 and 6 events exhibit a strong impulsive emission lasting for less than $100\,s$. A longer time scale initial peak is observed for June 9, and in the June 11 event, the rise is even slower. All four

Fig. 5.— Probability contours for the coefficients of the pion and bremsstrahlung components for spectral fits on Figure 4. The values of the coefficients are relative to the values used in Figure 3.

profiles show a slow, secondary increase following the initial peaks. The *TASC* is sensitive to all types of radiation, including solar neutrons whose arrival is delayed by the time-of-flight from the Sun. The secondary rise might be due in part to neutrons that were produced in the impulsive phase, but the time profiles cannot be completely accounted for in this manner with reasonable choices of power law production spectra. Moreover, the dip in the count rate that follows the initial peaks at about 300 to 400 s suggests the initial high energy neutron flux is small. Alternately, the secondary rise could signify an additional acceleration phase, or from neutron emission that is delayed from the flash phase.

A recent analysis by Mandzhavidze et al. 1996 based on the time profiles of the line emission in the *COMPTEL* (Ryan et al. 1993 and Murphy et al. 1993) and in the *EGRET TASC* in the 1991 June 11 event concluded that episodic acceleration and subsequent trapping of protons in low density regions accompanied by interactions in the denser sub-coronal regions could account for the data. Their analysis identified three distinct emission phases characterized by spectral variations in which the solar proton spectrum was harder during the second phase from about 130 to 170 min. The profiles shown in Figure 6 fall entirely

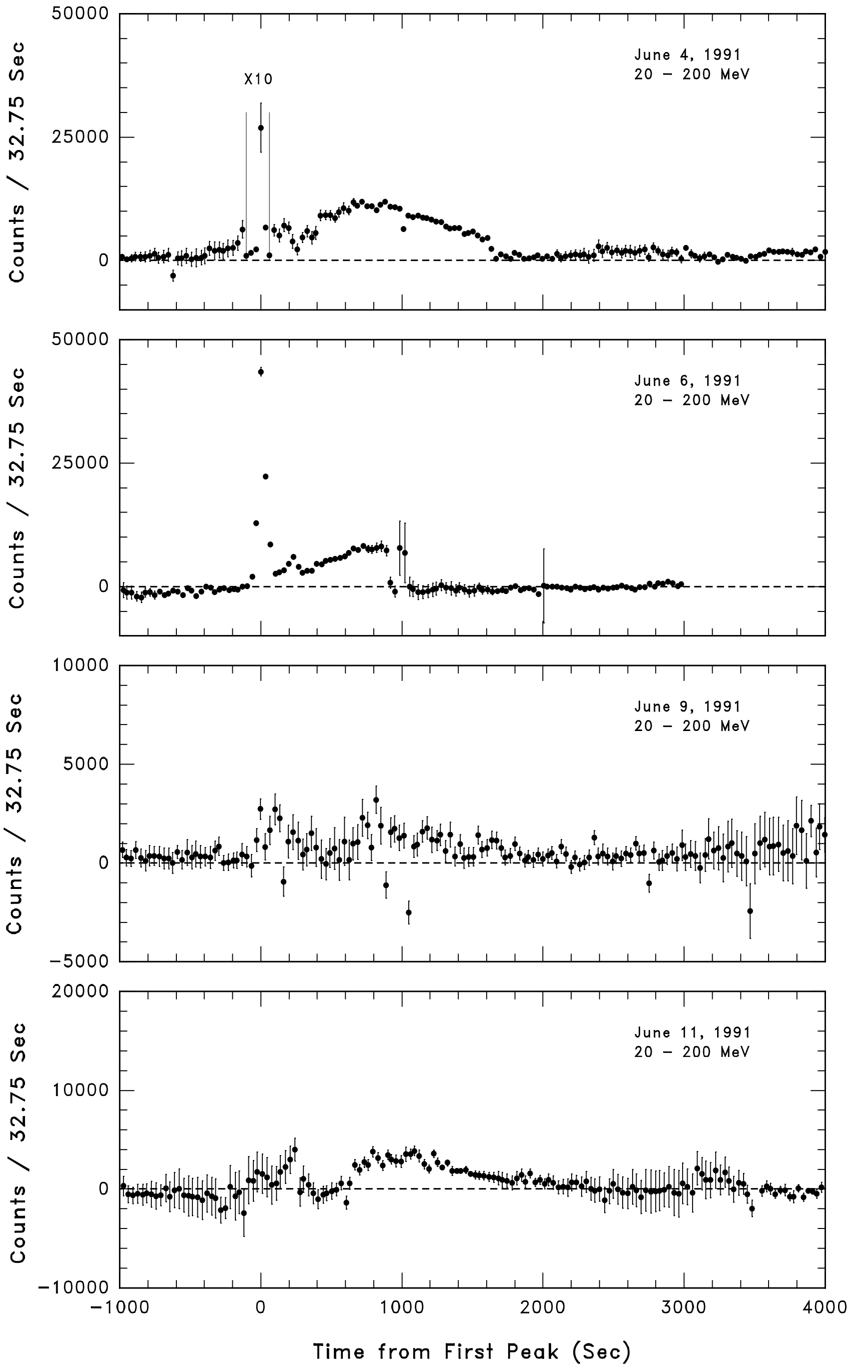

Fig. 6.— Time profiles of the count rate for the energy region of the *TASC* range for the 1991 June flares. The initial peak in the June 4 event, separated by vertical bars was reduced by $\times 10$ for presentation. Background rates have been subtracted.

within the first phase suggested by Mandzhavidze et al. 1996.

The *TASC* detector does not have active shielding and consequently it has a large background from charged particle radiation from all directions of incidence. Spectra from similar orbit locations before and after the spectrum of interest are used to determine and subtract this background. Converting the corrected counts spectrum to incident flux requires extensive modeling. For the first step in the process, a model input spectrum is chosen that is comprised of (1) two power laws, one for electron bremsstrahlung, and the other for remaining high energy emission, (2) a solar $2.22\,MeV$ neutron capture line, (3) a template of solar nuclear lines (Murphy et al. 1990), (4) and a secondary Fe line complex induced by neutron capture in the spacecraft. Then the model distribution is then propagated through the material of the spacecraft in the direction of the source using the *CGRO* mass model and EGS4 radiation transport codes. The resultant spectrum is folded with the *TASC* energy response function and then compared with the observations. The process is repeated until the input parameters describing the power laws and spectral line normalizations best match the data. Figure 7 shows an example of the components fit to the June 4 event at a time near the maximum of the secondary increase shown in Figure 6.

Figure 8 shows the results of fitting the model to all four of the 1991 June events in the early phases of each event. Notice that the sum of the model components, shown as a solid line fits the data very well. Line structure is evident in all four events. For the first two, the energy resolution of the lines is degraded by the large amount of spacecraft material in the path toward the Sun, while in the case of the last two, the instrument was pointed at the Sun and in these cases only minimal material exists in the path. All four events show a similar time evolution. Initially the steeper bremsstrahlung power law dominates over the hard power law. Then after the impulsive phase, the hard spectrum grows in importance and dominates the soft component. Later both power law components subside and eventually, the soft component again dominates. The neutron induced Fe lines are not present initially. They grow in significance during the times of the secondary rises shown in Figure 6 to levels typified in Figure 7 and then slowly decrease. This is evidence that at least part of the high energy increase is due to solar neutrons whose production is perhaps extended beyond the injection phase. Other evidence of solar neutron emission in the 1991 June flares is available. On June 4, ground-based measurements (Chiba et al. 1992) observed the arrival of energetic ($> 10\,\mathrm{GeV}$) neutrons that extended in time beyond the period expected if they were generated during the impulsive phase. *COMPTEL* (Ryan et al. 1992, Ryan et al. 1993) observed neutrons from the June 9 flare that were correlated with the impulsive phase with only a hint of continued production of neutrons. Detailed work on the evolution of the neutron capture lines and the delayed increase in Figure 6 is still in progress in an effort to determine the nature and extent of the solar neutron emission in these four flare events.

Fig. 7.— Model fits to the *TASC* data in the 1991 June 4 flare at a time near the secondary maximum shown in Figure 6. The components shown here have been modified by propagation through the spacecraft material and have been folded with the energy response function of the *TASC*. The double-dot-dash curve represents the power law that is similar to the bremsstrahlung component. The long dash signifies the second power law. The fine dash curve is the solar $2.22\,MeV$ neutron capture line. The dash-dot curve shows the solar C and O line complex. The medium dash curve shows the secondary Fe line complex that is induced by neutron capture in the spacecraft material. Finally, the total of the components is shown by the solid line.

The $> 50\,MeV$ flux for June 11 is shown in Figure 2 where it is noteworthy that the two independent spark chamber and *TASC* measurements of intensity are consistent and complementary. Figures 9 shows the time histories for the derived 2.22 and $4.4\,MeV$ fluxes for all four flares. These values are consistent with those observed by *OSSE* for June 4 (Murphy et al. 1993), and the $2.22\,MeV$ profile agrees with the *COMPEL* observation in the June 11 event (Rank et al. 1996). These line fluxes do not show the general increase seen late in the event at high energies that is evident in the high energy time profiles (Figure 6), and this indicates either a hardening of the solar flare proton spectrum as a function of time or an increase in the bremsstrahlung relative to the nucleon component. The ratio of the 4.4 and $2.22\,MeV$ line fluxes can also be used to determine the accelerated ion spectral index

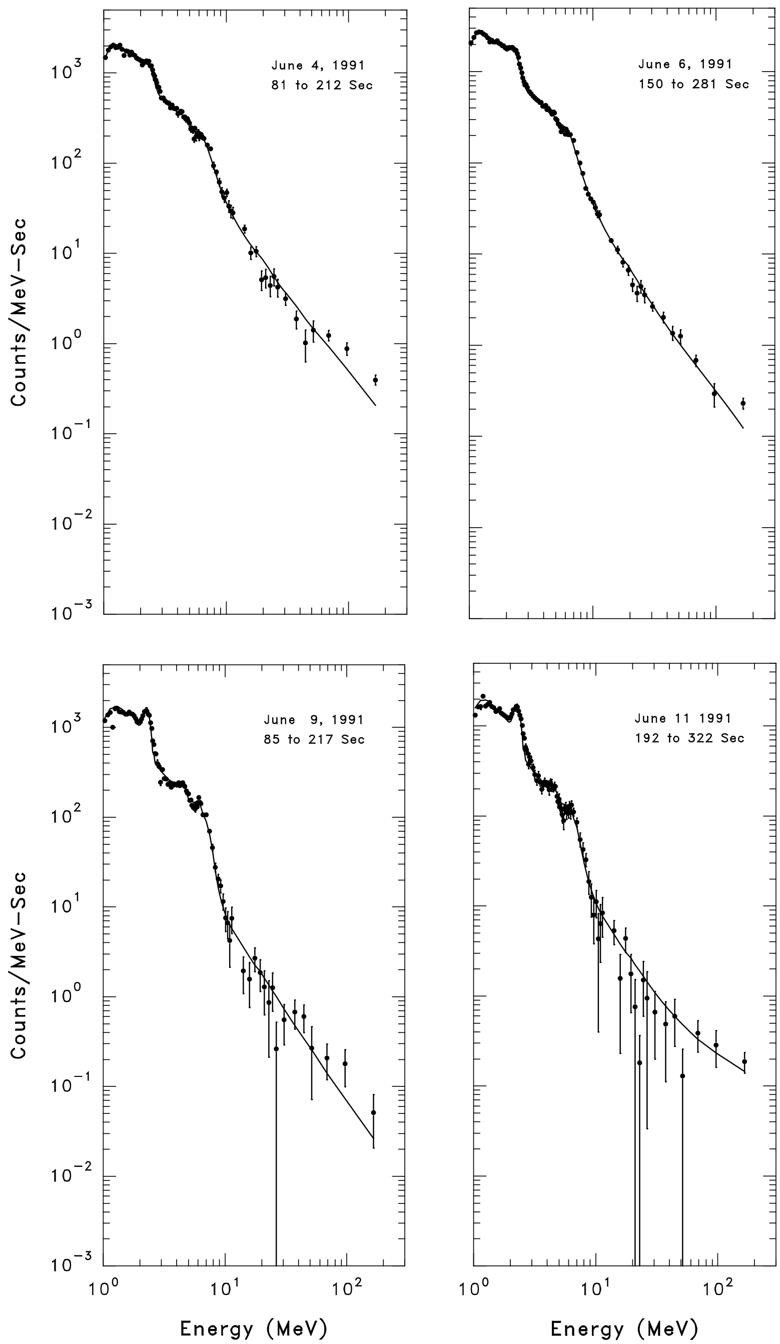

Fig. 8.— *TASC* spectra for the series of four 1991 June flare events at times that are near the impulsive phase. The solid line fits are the sum of the fitted components discussed in the text and shown in detail for the example in Figure 7.

(Ramaty and Murphy 1987). The proton index inferred from these results are generally in the range -3.5 to -3.0, consistent with the model spectrum discussed for Figure 3.

4.3. Summary

The *EGRET* observations of the intense flares during 1991 June provide significant new insights into the physics of flare particle acceleration and trapping. The flare on June 11 was particularly important in that the gamma ray spectrum extends to at least $2\,GeV$ – higher than any previous flare – when it was first observed $80\,min$ after the flash phase. If the *EGRET* anticoincidence shield had not been initially saturated and an earth occultation of the Sun had not occurred early in the event, it is likely that even higher energy emission would have been seen. This same event was also unique in its long time scale of over $8\,hr$. The relatively small class M5.3 flare that followed $18\,hr$ later produced a detectable increase (see Fig. 2.). It is unusual that such a small flare would be seen. This flare originated in the same region, but was 21° removed from the large flare. One possible speculation is that the efficiency for particle acceleration and gamma ray production is somehow increased in the conditions generated by the large flare. The energy spectrum indicates that both protons and electrons were accelerated in flare, and the subsequent time evolution indicates that the electron component does not decay more rapidly than the nuclear component, and in fact it appears to have a longer lifetime. This time behavior and the slow decay rate implies that the acceleration must be ongoing. Either it is continuous or it is episodic and accompanied by a trapping process rather than being a single flash acceleration followed by a very efficient trapping.

The *TASC* is not as sensitive as the spark chamber owing to its high background, but it did not suffer from significant saturation and was able to provide valuable information during about $1000\,s$ following the flash phase in all four of the large flares when the *EGRET* instrument was operational and the Sun was not occulted by the earth. The flares on June 4 and 6 had a much stronger impulsive phase than the flares on June 9 and 11, but otherwise they were very similar as viewed by the *TASC*. All four have clear evidence of neutron capture lines at $2.22\,MeV$ and lines in the C and O complex superimposed on a continuum. The continuum is modeled by two power laws; one, a soft component for bremsstrahlung and hard another for gamma rays produced by nuclear interactions at the Sun. Another series of lines in the Fe complex is also seen. The time evolution of these components in all four flares shows that relative to the bremsstrahlung emission, the nuclear component grows and then declines. The neutron induced Fe lines from the spacecraft material are not present initially and later grow to significance at the same time that the high energy portion

Fig. 9.— Time history of the 2.22 and 4.4 MeV lines in the four flare events observed by $EGRET$ in 1991 June. Values given for the total flux are integrated over the time interval of the data shown.

of the *TASC* emission time profile shows and increase. Consequently, neutron emission is a common feature of all four flares, and further analysis is being done using observed responses of NaI to machine-generated neutrons in an effort to unfold the neutron signal. The time profiles seem to require that the neutrons must be produced beyond the flash phase, and since the propagation delay for neutrons is energy dependent, the unfolding is model is time-dependent. Finally, the time profiles of the 2.22 and 4.4 MeV lines was determined, and their ratio is useful in estimating the proton spectral index at the Sun. For the values observed, the index is in the range -3.0 to -3.5 (Ramaty and Murphy 1987) that is in agreement with the fit to the high energy spectrum.

The *EGRET* instrument is expected to be functioning well into the next solar cycle even though much of the consumable spark chamber gas has been used. It is planned that some of the capability of the high energy spark chamber detector will be reserved for large solar events. The energy calorimeter does not require any consumables, and it will provide data similar to that reported in this paper for major flares of the new cycle.

4.4. Acknowledgements

The *EGRET* Team gratefully acknowledges support from the following: Bundesministerium für Forschung und Technologie, grant 50 QV 9095 (MPE); by the Deutsche Forschungsgemeinschaft (Sonderforschungsbereich 328) (Heidelberg); NASA grant NAG 5-1742 (HSC); NASA grant NAG 5-1605 (SU); and NASA contract NAS 5-31210 (GAC).

REFERENCES

Akimov, V. V. et al. 1991, 22nd Internat. Cosmic Ray Conf. Papers (Dublin, Ireland), 3, 73

Chiba N. et al. 1992, Astroparticle Physics, 1, 27

Chupp, E. L. 1984, ARA&A, 22, 359

Chupp, E. L. et al. 1973, Nature, 241, 333

Dunphy, P. P. & Chupp, E. L. 1991, 22nd International Cosmic Ray Conference (Dublin, Ireland), 3, 65

Dunphy, P. P. & Chupp, E. L. 1994, in High Energy Solar Phenomena–A New Era of Spacecraft Measurements, eds. J. Ryan & T. Vestrand, (Waterville, NH), AIP Conf. Proc., 294, 112.

Forman, M. A., Ramaty, R., & Zweibel, E. G. 1986, in Physics of the Sun, ed. P. A. Sturrock et al., Vol II (Dordrecht: Reidel), p. 249

Forrest, D. J. et al., 1980, Sol. Phys., 65, 15

Forrest, D. J. & Murphy, R. J. 1988, Sol. Phys., 118, 123

Forrest, D. J., Vestrand, W. T., Chupp, E.L., Rieger, E., Cooper, J., & Share, G. 1986, Adv. Space Res., 6,115

Hartman, R., et al. 1991, in The Compton Observatory Science Workshop, eds. C. Shrader, N. Gehrels, & B. Dennis, NASA-CP 3137, 116

Hua, X. & Lingenfelter, R. E. 1987, Sol. Phys., 107, 351

Hua, X. M., Ramaty, R., & Lingenfelter, R. E. 1989, ApJ, 341, 516

Hughes, E.B., et al. 1980, IEEE Trans. Nucl. Sci., NS-27, 364

Johnson, N., et al. 1993, ApJS, 86, 693

Kanbach, G., et al. 1988, Sp. Sci. Revs., 49, 69

Kanbach, G., et al. 1989, in Proc. Gamma Ray Observatory Science Workshop, GSFC, 2-1.

Kanbach, G. et al. 1993 A&ASuppl. 97, 349

Leikov, N. G. et al. 1993, A&ASuppl. 97, 345

Lingenfelter, R. E., Flamm, E. J., Canfield, E. H., & Kellman, S. 1965, J. Geophys. Res., 70, 4077

Mandzhavidze, N. & Ramaty, R. 1992, ApJ, 389, 739

Mandzhavidze, N. & Ramaty, R. 1992, ApJ, 396, L111

Mandzhavidze, N. and Ramaty, R. 1995, private communication

Mandzhavidze, N., Ramaty, R., Bertsch, D., and Schneid, E. 1996, in Proceedings of the High Energy Solar Physics Workshop, eds. R. Ramaty, N. Mandzhavidze, and X. Hua, (Greenbelt, MD), AIP Conf. Proc., 374, 225

Miller, J. A., Guessoum, N. & Ramaty, R. 1990, ApJ, 361, 701

Miller, J. A. & Ramaty, R. 1989, ApJ, 344, 973

Murphy, R. J. et al. 1993, in High Energy Solar Phenomena–A New Era of Spacecraft Measurements, eds. J. Ryan & T. Vestrand, (Waterville, NH), AIP Conf. Proc., 294, 15

Murphy, R. J., Dermer, C. D., & Ramaty, R. 1987, ApJS, 63, 721

Murphy, R. J., Share, G. H., Letaw, J. R. & Forrest, D. J. 1990 ApJ, 358, 298

Okudaira, K., Hirasima, Y., Yoshimori, M., & Kondo, I. 1981, 17th Int. Cosmic Ray Conf., (Paris, France), 3, 11

Ramaty, R. J., Kozlovsky, B., & Lingenfelter, R. E. 1975, Space Sci. Rev. 18, 341

Ramaty, R. and Mandzhavidze, N. 1994, in Proc. of the Kofu Symposium, eds. S. Enome and T. Hirayama, Nobeyama Radio Observatory Report No. 360, 275

Ramaty, R. & Murphy, R.J. 1987, Space Sci. Revs., 45, 213

Rank, G. et al. 1993, in High Energy Solar Phenomena–A New Era of Spacecraft Measurements, eds. J. Ryan & T. Vestrand, (Waterville, NH), AIP Conf. Proc., 294, 100

Rank, G. et al. 1996, in Proceedings of the High Energy Solar Physics Workshop, eds. R. Ramaty, N. Mandzhavidze, and X. Hua, (Greenbelt, MD), AIP Conf. Proc., 374, 219

Rieger, E. 1991, in Gamma-Ray Line Astrophysics; Proceedings of the International Symposium (Paris, France), eds. Ph. Durouchoux & N. Prantzos, New York, AIP, 421

Rieger, E. & Marschhauser, H. 1990, in Max91 SMM Solar Flares: Observations and Theory, eds. R. M. Winglee & A. L. Kiplinger, Proc. of the Max91 Workshop, (Estes Park, Co.), 3, 68

Ryan, J. et al. 1992, in Compton Gamma Ray Observatory Conference Proceedings, eds. M. Friedlander, N. Gehrels, & D. Macomb, (St. Louis, Mo.), AIP, 280, 631

Ryan, J. et al. 1993, in High Energy Solar Phenomena–A New Era of Spacecraft Measurements, eds. J. Ryan & T. Vestrand, (Waterville, NH), AIP Conf. Proc., 294, 89

Ryan, J. M. & Lee, M. A. 1991 ApJ, 368, 316

Schneid, E. et al. 1993 in High Energy Solar Phenomena–A New Era of Spacecraft Measurements, eds. J. Ryan & T. Vestrand, (Waterville, NH), AIP Conf. Proc., 294, 94

Schneid, E., et al. 1996, ApJ, 453, 95

Thompson, D. J. et al. 1993, ApJS, 86, 629

Trottet, G. et al. 1993, A&ASuppl. Ser. 97, 337

Vestrand, W. 1994, private communication.

Yoshimuri, M., 1990, ApJS, 73, 227

Yoshimuri, M., Okudaira, K., Hirasima, Y., & Kondo, I. 1983, Sol. Phys., 86, 375

æ